Coherent optical creation of a single molecule

Yichao Yu,[1, 2, 3, *] Kenneth Wang,[1, 2, 3] Jonathan D. Hood,[4] Lewis R. B. Picard,[1, 2, 3] Jessie T. Zhang,[1, 2, 3]
William B. Cairncross,[2, 1, 3] Jeremy M. Hutson,[5] Till Rosenband,[1] and Kang-Kuen Ni[2, 1, 3, †]

[1]*Department of Physics, Harvard University, Cambridge, Massachusetts 02138, USA*
[2]*Department of Chemistry and Chemical Biology, Harvard University, Cambridge, Massachusetts 02138, USA*
[3]*Harvard-MIT Center for Ultracold Atoms, Cambridge, Massachusetts 02138, USA*
[4]*Department of Chemistry, Purdue University, West Lafayette, Indianna, 47906, USA*
[5]*Joint Quantum Centre Durham-Newcastle, Department of Chemistry,
Durham University, Durham, DH1 3LE, United Kingdom*
(Dated: December 7, 2020)

We report on coherent association of atoms into a single weakly bound NaCs molecule in an optical tweezer through an optical Raman transition. The Raman scheme uses a deeply bound electronic excited intermediate state to achieve a large transition dipole moment while reducing photon scattering. Starting from two atoms in their relative motional ground state, we achieve an optical transfer efficiency of 69%. The molecules have a binding energy of 770.2 MHz at 8.83(2) G. This technique does not rely on Feshbach resonances or narrow excited-state lines and may allow a wide range of molecular species to be assembled atom-by-atom.

Diverse species of fully quantum controlled ultracold molecules are desired for a variety of applications including precision measurements [1–6], quantum simulations [7–10], quantum information processing [11–14], and studies of ultracold chemistry [15–18]. While many innovative approaches in the last few years have directly cooled different species of diatomic or polyatomic molecules below 1 mK [19–24], the highest phase-space-density gas [25] and trapped individual molecules [26, 27] have been achieved through the association of ultracold atoms.

Molecular association of ultracold atoms takes advantage of the cooling and trapping techniques that have been developed for atoms. Associating atoms into deeply bound molecules is challenging because of the small wavefunction overlap between the free-atom and molecular states and the release of a large amount of binding energy. A widely used method of overcoming these challenges is to associate atom pairs into weakly bound molecules first, and then transfer the molecules from this single internal state to a desired rovibrational and electronic state, releasing the binding energy by stimulated emission [1, 28–35]. So far, molecular association has generally been achieved by magnetoassociation through a magnetic Feshbach scattering resonance. Exceptions include Sr_2, where narrow linewidth (~ 20 kHz) excited states are available and optical association can be driven coherently [36, 37], and $^{87}Rb^{85}Rb$, where there are molecular states bound by $1 - 2$ MHz [27]. With these requirements, molecules involving non-magnetic atoms or atoms without narrow intercombination lines remain difficult to associate.

Here, we demonstrate coherent association of an atom pair to a weakly bound molecule by two-photon optical Raman transfer via an electronic excited state, as shown in Fig. 1a. The scheme does not rely on a Feshbach resonance, molecular states bound by a few MHz, or a narrow

excited state. The resulting single molecule is in a well-defined internal quantum state and predominantly in its motional ground state. A vibrational state of the electronic excited state $c^3\Sigma^+(\Omega = 1)$ serves as the intermediate state in the Raman scheme, and is chosen to minimize photon scattering during Raman Rabi oscillations. To reduce photon scattering and sensitivity to laser intensity noise further, we choose the initial and final states to balance the two Rabi frequencies as much as possible. This approach applies to a variety of molecules that can be created atom-by-atom with full quantum state control.

The optical Raman transfer is illustrated by the idealized three-level system shown in Fig. 1a, where the initial atomic state and the target weakly bound molecular state are coupled to an intermediate state by two lasers with Rabi frequencies Ω_a and Ω_m with one-photon detuning Δ, and all Rabi frequencies are population oscillation frequencies. The transfer Raman Rabi Rate is given by $\Omega_a\Omega_m/(2\Delta)$ [38]. Unlike Raman transitions in atoms, the two Rabi frequencies are greatly imbalanced ($\Omega_a/\Omega_m \ll 1$) due to the small wavefunction overlap between the atomic state and the intermediate state, and scattering losses are dominated by the final state. Furthermore, the energy difference between the atomic state and target molecular state is small (< 1 GHz) compared to the single-photon detuning Δ of 80 to 200 GHz, causing the target molecular state to scatter both beams nearly equally with a total rate $\Gamma_e\Omega_m^2/(2\Delta^2)$, where Γ_e is the excited-state linewidth [39]. In this idealized treatment, the ratio between the Raman Rabi frequency and the scattering rate is $\Omega_a/\Omega_m \times \Delta/\Gamma_e$, which limits the transfer efficiency into the molecular state. At the same time, the intensity-stability requirement is determined by the ratio of Raman Rabi frequency to light shift (Ω_a/Ω_m) [40]. Notably, both figures of merit improve with a larger ratio Ω_a/Ω_m.

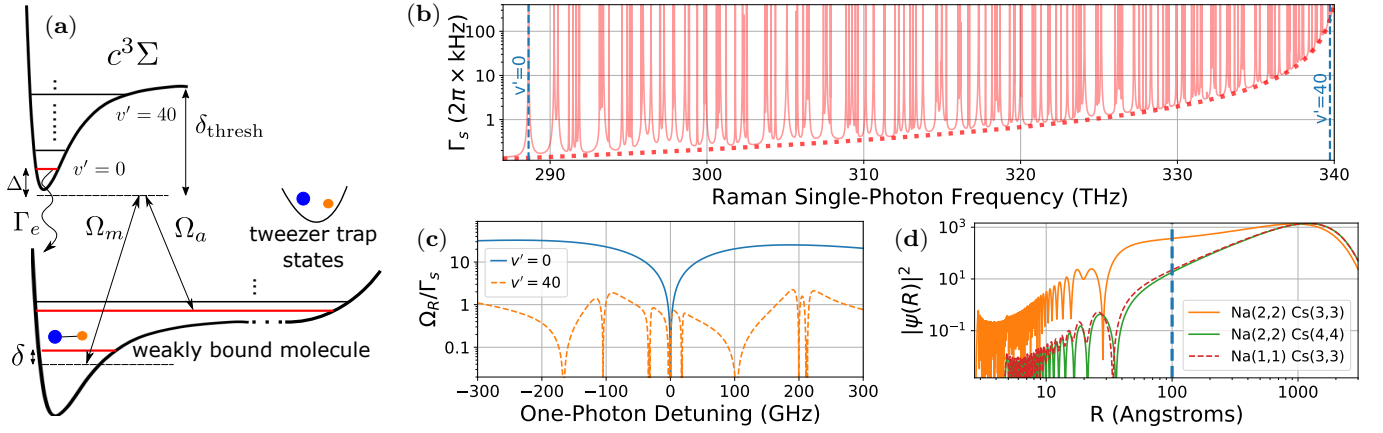Earlier experiments used weakly bound excited states

FIG. 1. Optical creation of single molecule from single atoms in tweezer. (a) Schematic of the optical transition from an atom pair to a weakly bound molecule. The initial state is the relative motional ground state between the two atoms and the final state is the first molecular bound state. The transition is driven by a pair of laser frequencies whose difference matches the binding energy of the molecule. The lasers are detuned from an excited molecular state in the $c^3\Sigma$ potential by Δ in order to suppress scattering during the transfer. (b) Comparison between weakly-bound and deeply-bound intermediate excited state for the Raman transition. The deeply bound excited state (blue lines $v'=0$) has a larger ratio of Raman Rabi frequency to scattering rate compared to the weakly bound excited state (orange lines $v'=40$) at a most detuning. (c) Enhancement of the short-range wavefunction. The large scattering length for the Na$(2,2)$, Cs$(3,3)$ state creates an interaction shift comparable to the axial trapping frequency. This causes a significant change in the relative wavefunction, especially at short internuclear distance (R). Compared to other spin states with weaker interaction, the wavefunction at short distance ($R < 100$ Å, left of the dashed line) is significantly enhanced.

as the intermediate state in the Raman transition to ensure a large Raman Rabi frequency [41, 42]. However, a complete picture includes both the many vibrational levels of the excited electronic state and the atomic continuum. The total scattering rate and Raman Rabi rate become a sum of the scattering rates and Raman Rabi rates over all possible intermediate states. As there is large overlap between the target molecular state and weakly bound excited states, intermediate states that are closer to the dissociation threshold result in a large scattering rate. This scattering is approximately proportional to $1/\delta_{\text{thresh}}^2$, where δ_{thresh} is the detuning from the dissociation threshold, which is smaller for intermediate states that are deeply bound [43]. [[TR1: Cite supplement or maybe Fig. S1 can go into Fig. 1b since it shows $\Gamma_s \sim \delta_{thresh}^{-2}$ nicely.]].

We optimize over intermediate states by calculating the Raman Rabi frequency Ω_R and scattering rate Γ_s at different detunings from the atomic threshold, taking into account of all states of 8 excited molecular potentials [44–48] and the continuum [49]. This calculation shows that the figure of merit Ω_R/Γ_s can be larger for more deeply bound states compared to weakly bound states at a cost of a smaller transfer rate Ω_R, as shown in Fig. 1b; see Supplementary Material for details. As a result, we choose the $v'=0$ level of $c^3\Sigma^+(\Omega=1)$ as the intermediate state near which to drive Raman transitions.

In addition to the intermediate state, the choice of initial and final Zeeman and hyperfine states affects the single-photon rates Ω_a and Ω_m. Due to the small extent of the intermediate-state wavefunction compared to that of the trapped atoms, Ω_a is approximately proportional to the amplitude of the relative atomic wavefunction at short distance, within the range of the molecular potential. To increase this amplitude, one can increase the external confinement of atom pairs. In a harmonic approximation the short-range amplitude is proportional to $\omega_{\text{trap}}^{3/4}$ or $P^{3/8}$, where ω_{trap} is the trap frequency and P is the optical power in the tweezer trap [50] with a fixed beam waist. However, additional power may not be available and also leads to additional undesired scattering. Alternatively, one can choose an atomic pair state with a large scattering length (positive or negative). For such states, the amplitude of the relative atomic wavefunction is substantially enhanced at short range, as shown in Fig. 1c. For our system of Na and Cs atoms, we choose a spin-state combination $|\uparrow_{\text{Na}}\downarrow_{\text{Cs}}\rangle \equiv |f=2, m_f=2\rangle_{\text{Na}} |f=3, m_f=3\rangle_{\text{Cs}}$ that has a large and negative scattering length of $a(\uparrow_{\text{Na}}\downarrow_{\text{Cs}}) \approx -700 a_0$ [51]. All other stable spin combinations give smaller scattering lengths ($< 50 a_0$).

To identify a suitable target molecular state, we carry out coupled-channel calculations of the near-threshold bound states, as described in the Supplemental Material. Choosing a bound state with similar spin character to the atomic state minimizes the sensitivity of the transition frequency to magnetic field. A suitable state with this character is predicted about 763 MHz below the $|\uparrow_{\text{Na}}\downarrow_{\text{Cs}}\rangle$ threshold and the ratio Ω_a/Ω_m increases to

FIG. 2. Beampath for generating the frequency for Raman transition in the tweezer. (Some mirrors and other optics used for alignment are not included.) The two ASE filters before and after the fibers are also shown. The laser source is a fiber amplifier seeded by a external cavity diode laser. The red beam path is the 0-th order of the double pass (DP) AOM which is used for the tweezer. When the double-pass (DP) AOM is turned on, some power is redirected to the first order (blue beam path) which generates the required frequency different to drive the Raman transition. The two frequencies are recombined on the DP AOM. The 0-th order light is shifted by another single pass (SP) AOM running on a different frequency before recombining. Without this AOM, the leak light from the DP AOM will be at the same frequency as the 0-th order light which can cause a significant power fluctuation due to interference. The experiment typically start with the SP AOM on and the DP AOM off. When driving the Raman transition, the powers on both AOMs are ramped simultaneously to achieve the desired power at both frequencies.

FIG. 3. Coherent transfer of atoms to molecules. The molecular state is dark to the imaging step and corresponds to zero signal. (a) Raman difference frequency scans for various durations showing the resonance as a frequency offset from 770.2 MHz, near the calculated value of 763 MHz. (b) Raman pulse-length scan on resonance. A decaying Rabi oscillation shows the coherence of the Raman transfer process. A model is fitted to (a) and (b) to determine the Raman Rabi frequency and loss rates. *Inset:* Geometry and polarization of trap and Raman beam relative to the magnetic field. The X.yy mW beam is focused to a waist of 0.9 μm that confines the atoms and molecule. A perpendicular $B_0 = 8.83(2)$ G magnetic field defines the quantization axis and the atoms experience predominantly π-polarized light.

about 0.013. Compared to $\Omega_a/\Omega_m \approx 0.003$ for other combinations, this relaxes the intensity stability requirement to the percent level and enhances the Raman Rabi frequency.

Experimentally, we first prepare two atoms in a well-defined external and internal quantum state by using techniques developed previously [52–54]. In brief, the experimental cycle begins by stochastically loading a single ^{23}Na atom and a single ^{133}Cs atom into separate optical tweezers. The atoms are initially imaged to distinguish between loading of two atoms, one atom (Na or Cs), or no atom to be able to post-select from the experimental results based on the initial loading condition. After imaging, we turn on a 8.83(2) G magnetic field to define the quantization axis for the state preparation and molecule formation steps. Raman sideband cooling is then applied to prepare both atoms simultaneously in the 3-dimensional motional ground state of their optical tweezers, leaving the atoms in the spin state $|\uparrow_{Na}\uparrow_{Cs}\rangle \equiv |f = 2, m_f = 2\rangle_{Na} |f = 4, m_f = 4\rangle_{Cs}$, which has a small scattering length. The weak two-atom interaction allows merging of the two tweezers with minimum pertubation so that they remain in the motional ground state.

Next, we drive the atoms into spin combination $|\uparrow_{Na}\downarrow_{Cs}\rangle$ with a large scattering length by performing a Cs spin flip while taking into account the -30.7 kHz interaction shift [51]. This is the initial atomic state for Raman transfer. The spin flip selectively transfers atoms in the relative motional ground state, removing any background from atoms in excited motional states [55]. For the experiment reported here, 31% of initial two-atom population is transferred.

To transfer the atom pair into the target weakly bound molecular state, we modulate the tweezer beam with a
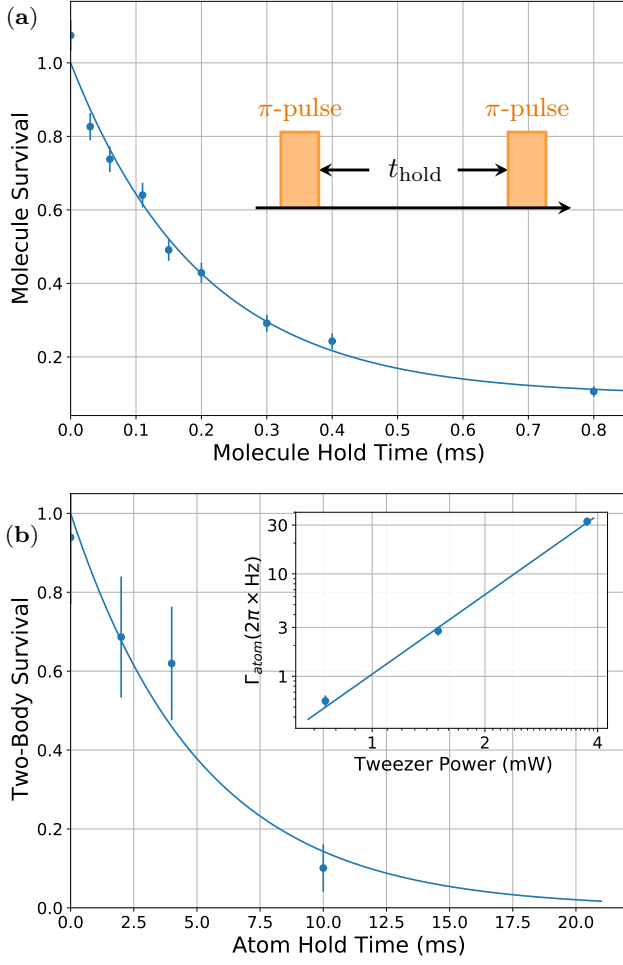
FIG. 4. (a) Direct measurement of molecule lifetime with about $X.XX$ mW optical power. Molecule survival is detected by dissociating back to atoms via a second Raman transition. The lifetime is consistent with the 0.199(9) ms measured from the Raman transition data. Inset: pulse sequence for the lifetime measurement. (b) Two-body atom lifetime of 5(1) ms in a trap of depth $X.XX$ mW caused by off-resonance photoassociation. This is used to improve the fitting of the Raman transfer data. Inset: Atomic scattering rate scales as $P_{tweezer}^{2.58} \times 2\pi \times 29.3(17)$ mHz/mW$^{2.58}$ on a log-log scale; this is consistent with a two-photon scattering process. We have not measured a clear dependency of the loss rate on the tweezer detuning.

second frequency near 770 MHz, as shown in Fig. 2. The dual use of the tweezer beam for confinement and Raman transfer not only minimizes photon scattering, but also allows a tight focus to minimize the transfer duration. A tweezer frequency far detuned (by -151 GHz) from $v' = 0$ (< 50 MHz natural linewidth) reduces resonant scattering [53].

Figure 3 shows a Fourier-limited resonance together with Rabi oscillations between the atomic and molecular states. A decaying Rabi oscillation with frequency

$2\pi \times 3.28(4)$ kHz fitted to the data suggests that 69 % of atoms initially in the relative motional ground state are transferred into the molecular state after a π-pulse. Over 60% of the molecules are in the motional ground state (both relative and center of mass), inferred from independent Raman sideband thermometry measurements of the atoms.

To better understand the details and limitations of the Raman transfer process, we measured the properties of the two-photon resonance as a function of tweezer power and single-photon detuning. Known dependencies of the light shift and Raman Rabi frequency on detuning Δ allow experimental determination of the Rabi frequencies Ω_a and Ω_m whose ratio critically affects the transfer efficiency. Both the light shift and Raman Rabi frequency follow a $1/\Delta$ slope as shown in Fig. 5a, b and include a constant offset that we attribute to coupling to other excited states that are further away in energy. The $1/\Delta$ components, due to the nearby $v' = 0$ intermediate state, determine Ω_m and Ω_a in from the fit coefficients, as shown in Table I.

P (mW)	0.75	1.5	3.75
f_{PA0} (GHz)		288711.8	
a ($2\pi \times$ MHz)	770.20452(6)	770.2081(1)	770.1943(3)
b ($4\pi^2 \times$ MHz $\cdot$ GHz)	$-12.46(2)$	$-24.44(3)$	$-60.66(8)$
c ($2\pi \times$ kHz)	0.29(2)	0.63(4)	2.4(2)
d ($4\pi^2 \times$ MHz $\cdot$ GHz)	0.115(4)	0.275(6)	0.95(3)
Ω_R ($2\pi \times$ kHz)	0.49(2)	1.18(3)	3.97(9)
Ω_m ($2\pi \times$ MHz)			348.3(3)
Ω_a ($2\pi \times$ kHz)			5.5(2)

TABLE I. Fitting results for Fig. 5(a,b). Ω_R is reported at -151 GHz detuning from the $v' = 0$ state. The coefficients Ω_m and Ω_a are in broad agreement with our calculation and their ratio at 3.75 mW is 0.016, which is near the theory prediction of 0.013. The measured Rabi rate Ω_R is ZZ % of $\Omega_m \Omega_a /(2\Delta)$ due to interference from further-detuned Raman processes.

We perform the experiment at various tweezer powers to extract the power dependence of Ω_m and Ω_a, as shown in Fig. 5c. Ω_m scales like $P^{1/2}$ as expected. As discussed previously, the scaling of Ω_a is $P^{7/8}$ for weakly interacting particles. However, due to the strong interaction between the two atoms in the $|\uparrow_{Na}\downarrow_{Cs}\rangle$ state, this approximation breaks down. Coupled-channel calculations show that the wavefunction scaling is well approximated by $P^{0.29}$ within the range of confinement in our experiment and the expected scaling of $\Omega_a \propto P^{0.79}$ agrees with the data.

The measured single-photon Rabi frequencies of Table I are in broad agreement with calculations (see Supplementary Materials). From the full calculation of the expected scattering rate including all excited states

Raman transfer efficiency is limited by the molecular lifetime, together with a reduction in the Raman Rabi
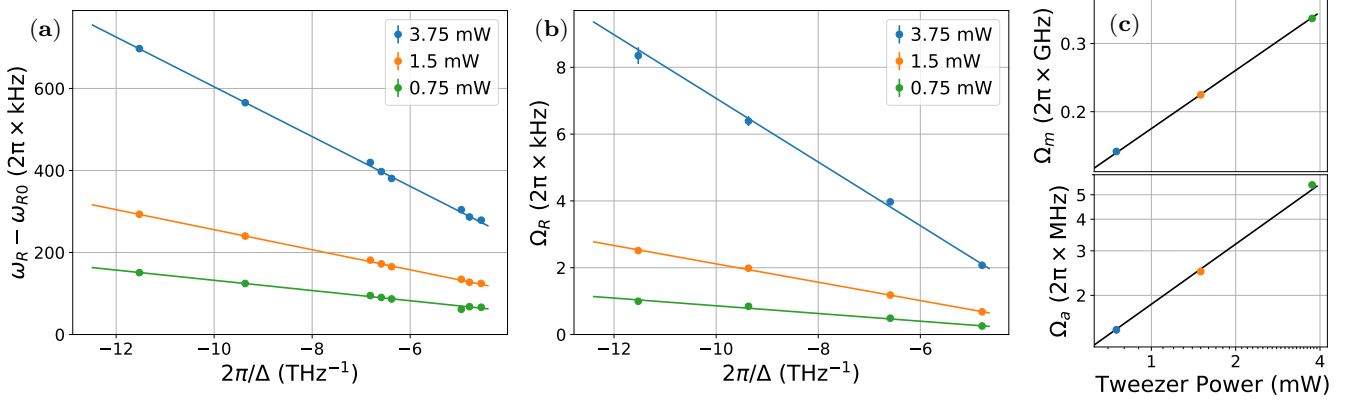
FIG. 5. Raman transition parameters as a function of tweezer power and detuning. (a) The Raman resonance fitted by $a_P + b_P/\Delta$, where a_P and $b_P = (\Omega_a^2 - \Omega_m^2)/2$ are the power (P) dependent background and $v' = 0$ contributions to the light shift and $\Delta \equiv 2\pi \times (f_0 - f_{\text{tweezer}})$ is the detuning from the $v' = 0$ resonance frequency f_0. a_P is fitted to a model including linear and small quadratic light shift to obtain the Raman resonance frequency at zero tweezer power $\omega_{R0} = 2\pi \times 770.1969(2)$ MHz where the statistical uncertainty is shown. (b) Raman Rabi frequency (Ω_R) fitted to $c_P + d_P/\Delta$, where c_P and $d_P = \Omega_a\Omega_m/2$ are the background and $v' = 0$ contributions that scale as $P^{1.29}$ with optical power. The detuning is calculated from the PA frequency fitted in (a). Fit parameters are listed in Table I. (c) Tweezer power dependency of Ω_m (top) and Ω_a (bottom) calculated from b_P and d_P on a log-log scale showing approximate $P^{0.5}$ scaling of Ω_m and $P^{0.79}$ scaling of Ω_a. [[TR: There should be a gap between (c) top and bottom.]

frequency due to destructive interference with intermediate states beyond v'=0 (see Table I). The lifetime is measured directly by preparing the molecule with a π-pulse, followed after a variable delay by a second dissociating π-pulse. The result in Fig. 4a shows a molecular lifetime of 0.199(9) ms, consistent with the decay of the Rabi oscillation in Fig. 3b. Preliminary experiments and theoretical considerations indicate that the molecular lifetime may be limited by two-photon coupling to the atomic continuum [56]. Atom loss is shown to be small in Fig. 4 by measuring the one- and two-body lifetimes of the atoms directly without the second Raman frequency. In principle, destructive interference that reduces the Raman Rabi rate for negative detunings Δ changes to constructive interference for positive detunings, but additional molecular resonances made the positive region unusable. Separately we observe a decrease in coherence by a factor of 2 without laser spectrum filters, suggesting that spectral impurity of the laser can be a significant source of loss.

Other potential decoherence sources include fluctuations of the tweezer intensity and magnetic field. Based on the Rabi frequency ratio in Table I the requirement on the tweezer intensity stability is 0.8% at 3.75 mW power. We stabilize the power to 0.1%, indicating that in the absence of beam-waist fluctuations, light shift is not a major source of decoherence. Similarly, the measured Zeeman shift of 42.2(2) kHz/G does not cause significant decoherence for the measured magnetic field fluctuation of 1.5 mG.

In conclusion, we have coherently formed a weakly

bound NaCs molecule in an optical tweezer by optical Raman transfer. This process is enabled by utilizing a deeply-bound intermediate state, as well as highly-interacting initial atomic states. A theoretical investigation including 8 excited state potentials, the excited atomic continuum, and coupled-channel ground state wavefunctions indicates the potential for higher transfer efficiency than the observed value of 69 %. Future experiments may benefit from better balancing of the up-leg and down-leg Rabi frequencies, for example by driving to more deeply bound states. If possible, destructive interference that reduces the two-photon Rabi rate should be avoided. Nonlinear optical effects that limit the molecular state lifetime can also be explored.

Our technique can be applied to form a diverse set of molecular species, because it does not rely on a magnetic Feshbach resonance, states bound by only a few MHz, or a narrow excited state. The formation of weakly bound molecules is a key step in forming rovibrational ground state molecules. By scaling up to many optical tweezers [57–59], large arrays with arbitrary geometry of highly controlled molecules can be achieved. These molecules comprise a flexible platform for quantum simulation and quantum computing applications. (End with a sentence on molecules for future quantum applications?)

[[TR2: Mention somewhere that the shape of Fig. 3b Rabi flopping indicates molecular loss, not atomic loss or frequency fluctuation.]]

[[TR3: Check all "$P = 3.75$ mW" results because they may negelect reduction from 2nd ASE filter. Better to quote the reduced power.]]

[[TR4: "We" is overused in this paper and obscures more important subject-object relationships. Authorship already implies that "we" did everything in the paper.]]

[[TR5: Is Raman Rabi freq the best term for Ω_R?]]

[[TR6: Broader statement on experimentally possible vs. theoretical detunings.]]

---

* yichaoyu@g.harvard.edu
† ni@chemistry.harvard.edu

[1] S. S. Kondov, C.-H. Lee, K. H. Leung, C. Liedl, I. Majewska, R. Moszynski, and T. Zelevinsky, Nature Physics **15**, 1118–1122 (2019).

[2] I. Kozyryev and N. R. Hutzler, Physical Review Letters **119**, 133002 (2017), publisher: American Physical Society.

[3] V. V. Flambaum and V. A. Dzuba, Phys. Rev. A **101**, 042504 (2020).

[4] V. Andreev, D. G. Ang, D. DeMille, J. M. Doyle, G. Gabrielse, J. Haefner, N. R. Hutzler, Z. Lasner, C. Meisenhelder, B. R. O'Leary, C. D. Panda, A. D. West, E. P. West, X. Wu, and A. C. M. E. Collaboration, Nature **562**, 355 (2018).

[5] W. B. Cairncross, D. N. Gresh, M. Grau, K. C. Cossel, T. S. Roussy, Y. Ni, Y. Zhou, J. Ye, and E. A. Cornell, Phys. Rev. Lett. **119**, 153001 (2017).

[6] J. J. Hudson, D. M. Kara, I. J. Smallman, B. E. Sauer, M. R. Tarbutt, and E. A. Hinds, Nature **473**, 493 (2011).

[7] A. Micheli, G. Brennen, and P. Zoller, Nat. Phys. **2**, 341 (2006).

[8] N. Y. Yao, M. P. Zaletel, D. M. Stamper-Kurn, and A. Vishwanath, Nature Physics **14**, 405 (2018).

[9] M. L. Wall, K. R. A. Hazzard, and A. M. Rey, From atomic to mesoscale: The role of quantum coherence in systems of various complexities (World Scientific, 2015) Chap. Quantum magnetism with ultracold molecules.

[10] M. Wall, K. Maeda, and L. D. Carr, New Journal of Physics **17**, 025001 (2015).

[11] D. DeMille, Phys. Rev. Lett. **88**, 067901 (2002).

[12] K.-K. Ni, T. Rosenband, and D. D. Grimes, Chem. Sci. **9**, 6830 (2018).

[13] E. R. Hudson and W. C. Campbell, Phys. Rev. A **98**, 040302(R) (2018).

[14] Y. Lin, D. R. Leibrandt, D. Leibfried, and C.-W. Chou, Nature **581**, 273 (2020).

[15] N. Balakrishnan, J. Chem. Phys. **145**, 150901 (2016).

[16] M.-G. Hu, Y. Liu, D. D. Grimes, Y.-W. Lin, A. H. Gheorghe, R. Vexiau, N. Bouloufa-Maafa, O. Dulieu, T. Rosenband, and K.-K. Ni, Science **366**, 1111 (2019).

[17] Y. Segev, M. Pitzer, M. Karpov, N. Akerman, J. Narevicius, and E. Narevicius, Nature **572**, 189 (2019).

[18] T. de Jongh, M. Besemer, Q. Shuai, T. Karman, A. van der Avoird, G. C. Groenenboom, and S. Y. T. van de Meerakker, Science **368**, 626 (2020), https://science.sciencemag.org/content/368/6491/626.full.pdf.

[19] E. B. Norrgard, D. J. McCarron, M. H. Steinecker, M. R. Tarbutt, and D. DeMille, Phys. Rev. Lett. **116**, 063004 (2016).

[20] L. Anderegg, B. L. Augenbraun, Y. Bao, S. Burchesky, L. W. Cheuk, W. Ketterle, and J. M. Doyle, Nature Physics **14**, 890 (2018).

[21] D. Mitra, N. B. Vilas, C. Hallas, L. Anderegg, B. L. Augenbraun, L. Baum, C. Miller, S. Raval, and J. M. Doyle, Science **369**, 1366 (2020).

[22] S. Ding, Y. Wu, I. A. Finneran, J. J. Burau, and J. Ye, Phys. Rev. X **10**, 021049 (2020).

[23] D. J. McCarron, M. H. Steinecker, Y. Zhu, and D. DeMille, Phys. Rev. Lett. **121**, 013202 (2018).

[24] S. Truppe, H. J. Williams, M. Hambach, L. Caldwell, N. J. Fitch, E. A. Hinds, B. E. Sauer, and M. R. Tarbutt, Nature Physics **13**, 1173 (2017).

[25] L. De Marco, G. Valtolina, K. Matsuda, W. G. Tobias, J. P. Covey, and J. Ye, Science **363**, 853 (2019).

[26] J. T. Zhang, Y. Yu, W. B. Cairncross, K. Wang, L. R. B. Picard, J. D. Hood, Y.-W. Lin, J. M. Hutson, and K.-K. Ni, Phys. Rev. Lett. **124**, 253401 (2020).

[27] X. He, K. Wang, J. Zhuang, P. Xu, X. Gao, R. Guo, C. Sheng, M. Liu, J. Wang, J. Li, G. V. Shlyapnikov, and M. Zhan, Science **370**, 331 (2020).

[28] J. G. Danzl, E. Haller, M. Gustavsson, M. J. Mark, R. Hart, N. Bouloufa, O. Dulieu, H. Ritsch, and H.-C. Nägerl, Science **321**, 1062 (2008).

[29] K.-K. Ni, S. Ospelkaus, M. H. G. de Miranda, A. Pe'er, B. Neyenhuis, J. J. Zirbel, S. Kotochigova, P. S. Julienne, D. S. Jin, and J. Ye, Science **322**, 231 (2008).

[30] F. Lang, K. Winkler, C. Strauss, R. Grimm, and J. Hecker Denschlag, Phys. Rev. Lett. **101**, 133005 (2008).

[31] T. Takekoshi, L. Reichsöllner, A. Schindewolf, J. M. Hutson, C. R. Le Sueur, O. Dulieu, F. Ferlaino, R. Grimm, and H.-C. Nägerl, Phys. Rev. Lett. **113**, 205301 (2014).

[32] P. K. Molony, P. D. Gregory, Z. Ji, B. Lu, M. P. Köppinger, C. R. Le Sueur, C. L. Blackley, J. M. Hutson, and S. L. Cornish, Phys. Rev. Lett. **113**, 255301 (2014).

[33] J. W. Park, S. A. Will, and M. W. Zwierlein, Phys. Rev. Lett. **114**, 205302 (2015).

[34] M. Guo, B. Zhu, B. Lu, X. Ye, F. Wang, R. Vexiau, N. Bouloufa-Maafa, G. Quéméner, O. Dulieu, and D. Wang, Phys. Rev. Lett. **116**, 205303 (2016).

[35] K. K. Voges, P. Gersema, M. Meyer zum Alten Borgloh, T. A. Schulze, T. Hartmann, A. Zenesini, and S. Ospelkaus, Phys. Rev. Lett. **125**, 083401 (2020).

[36] G. Reinaudi, C. B. Osborn, M. McDonald, S. Kotochigova, and T. Zelevinsky, Phys. Rev. Lett. **109**, 115303 (2012).

[37] S. Stellmer, B. Pasquiou, R. Grimm, and F. Schreck, Phys. Rev. Lett. **109**, 115302 (2012).

[38] D. J. Wineland, M. Barrett, J. Britton, J. Chiaverini, B. DeMarco, W. M. Itano, B. Jelenković, C. Langer,

D. Leibfried, V. Meyer, T. Rosenband, and T. Schätz, Philosophical Transactions of the Royal Society of London A: Mathematical, Physical and Engineering Sciences **361**, 1349 (2003).

[39] The two beams have equal power to maximize the Raman Rabi rate at fixed total power, resulting in a factor of 2 for scattering two beams.

[40] There is an additional factor of 2, with both beams at equal power, to account for the Stark shift caused by both beams.

[41] R. Wynar, R. S. Freeland, D. J. Han, C. Ryu, and D. J. Heinzen, Science **287**, 1016 (2000).

[42] T. Rom, T. Best, O. Mandel, A. Widera, M. Greiner, T. W. Hänsch, and I. Bloch, Phys. Rev. Lett. **93**, 073002 (2004).

[43] See Supplementary Material.

[44] M. Korek, S. Bleik, and A. R. Allouche, J. Chem. Phys. **126**, 124313 (2007).

[45] A. Grochola, P. Kowalczyk, J. Szczepkowski, W. Jastrzebski, A. Wakim, P. Zabawa, and N. P. Bigelow, Phys. Rev. A **84**, 012507 (2011).

[46] J. Zaharova, M. Tamanis, R. Ferber, A. N. Drozdova, E. A. Pazyuk, and A. V. Stolyarov, Phys. Rev. A **79**, 012508 (2009).

[47] A. Grochola, P. Kowalczyk, and W. Jastrzebski, Chemical Physics Letters **497**, 22 (2010).

[48] P. J. Zabawa, *Production of Ultracold, Absolute Vibrational Ground State NaCs Molecules*, Ph.D. thesis, University of Rochester (2012).

[49] L. R. Liu, J. T. Zhang, Y. Yu, N. R. Hutzler, Y. Liu, T. Rosenband, and K.-K. Ni, arXiv:1701.03121 (2017).

[50] F. H. Mies, E. Tiesinga, and P. S. Julienne, Phys. Rev. A **61**, 022721 (2000).

[51] J. D. Hood, Y. Yu, Y.-W. Lin, J. T. Zhang, K. Wang, L. R. Liu, B. Gao, and K.-K. Ni, Phys. Rev. Research **2**, 023108 (2020).

[52] L. R. Liu, J. D. Hood, Y. Yu, J. T. Zhang, N. R. Hutzler, T. Rosenband, and K.-K. Ni, Science **360**, 900 (2018).

[53] L. R. Liu, J. D. Hood, Y. Yu, J. T. Zhang, K. Wang, Y.-W. Lin, T. Rosenband, and K.-K. Ni, Phys. Rev. X **9**, 021039 (2019).

[54] K. Wang, X. He, R. Guo, P. Xu, C. Sheng, J. Zhuang, Z. Xiong, M. Liu, J. Wang, and M. Zhan, Phys. Rev. A **100**, 063429 (2019).

[55] This interaction shift is larger than the differential axial trapping frequency between Na and Cs atoms, which decouples the relative and center of mass motional state and improves the robustness of our preparation of the relative motional ground state.

[56] Y. Yu, *Coherent Creation of Single Molecuels from Single Atoms*, Ph.D. thesis, Harvard University (2021).

[57] M. Endres, H. Bernien, A. Keesling, H. Levine, E. R. Anschuetz, A. Krajenbrink, C. Senko, V. Vuletic, M. Greiner, and M. D. Lukin, Science **354**, 1024 (2016).

[58] D. Barredo, V. Lienhard, S. de Léséleuc, T. Lahaye, and A. Browaeys, Nature **561**, 79 (2018).

[59] D. Ohl de Mello, D. Schäffner, J. Werkmann, T. Preuschoff, L. Kohfahl, M. Schlosser, and G. Birkl, Phys. Rev. Lett. **122**, 203601 (2019).